





RESEARCH ARTICLE

[View Article Online](#)
[View Journal](#)


Cite this: DOI: 10.1039/d2qi01267g

Supramolecular gold(i) vesicles: an in-depth study of their aggregation process†

 Andrea Pinto, ^{a,b} Jaume Sonet,^a Rosa M. Gomila, ^c Antonio Frontera, ^c
 João Carlos Lima ^d and Laura Rodríguez ^{*a,b}

The synthesis of two gold(i) complexes containing a pyridyl ligand with a polyethyleneglycol pendant arm at one position and a chromophore (aniline or coumarin) at the second coordination position is herein reported. These compounds have been observed to aggregate in acetonitrile/water mixtures and the results have been compared with two other gold(i) compounds previously synthesized by our group that contain a water soluble phosphane instead of the pyridyl ligand. We observed that the coumarin derivative is much more stable while the aniline analogue decomposes in the presence of small amounts of water. The aggregation of this coumarin gold(i) compound has been deeply studied by DLS, SAXS, optical microscopy and electron microscopy (SEM and cryo-TEM). The calculation of the crystal packing parameter confirms a vesicle-type assembly. In order to obtain more detailed information about the composition of vesicles, the number of molecules involved in the self-assembly process has been determined ($N_{agg} = 82$). DFT calculations support these data, determining a size of around 90 Å for the vesicles, which may form coacervates to yield the larger structures observed under a microscope.

 Received 14th June 2022,
 Accepted 2nd September 2022

DOI: 10.1039/d2qi01267g

rsc.li/frontiers-inorganic

Introduction

The self-assembly of small molecules is a powerful bottom-up approach for the preparation of a wide variety of supramolecular structures and nanomaterials, which has received great attention in the past decade.^{1,2} It offers different advantages thanks to its reversibility, which can confer the ability of modification of different properties (output) upon reception of an external stimulus. This technologically relevant science has led many research groups to take advantage of non-covalent interactions in order to construct supramolecular structures with different morphologies and with specific functions and applications.^{3–6}

Within this field, gold(i) complexes are exceptionally appealing due to the well-known weak Au(i)⋯Au(i) interactions, being some of the strongest homometallophilic interactions that are comparable to hydrogen bonding.⁷ They can

be directly involved in the resulting assemblies and their properties^{8,9} having additional weak interactions that will modulate the resulting assemblies. In particular, small molecules containing a gold(i) alkynyl unit are attractive building blocks for the construction of organometallic materials due to the preference of gold(i) for a linear coordination geometry and the π -unsaturated nature of the acetylide unit. Other parameters, such as solvent polarity of the ionic *vs.* neutral character of the molecule, have also been observed to play a direct role in the self-assembly process.^{10–12}

Another approach to ensure the aggregation of small molecules is the introduction of an amphiphilic group in the chemical structure of the molecule. The arrangement of the molecules that contain this group is usually driven by hydrophilic and hydrophobic interactions that allow construction of supramolecular structures due to repulsive interactions with aqueous media. Poly(ethylene glycol) (PEG) is an amphiphilic moiety with a hydrophilic character that can favour the solubility of metal complexes in water. Moreover, its amphiphilic character ensures the resulting supramolecular assemblies through strong non-covalent interactions. This ligand has been barely used in organometallic chemistry although its resulting complexes may be useful in green chemistry and environmentally friendly applications thanks to the solubility of the molecules in water. Some applications in bioimaging,¹ catalysis¹³ or in controlling self-assembly with the aim of changing the luminescence properties have been described.^{14,15}

^aDepartament de Química Inorgànica i Orgànica, Secció de Química Inorgànica, Universitat de Barcelona, Martí i Franquès 1-11, E-08028 Barcelona, Spain.
 E-mail: laura.rodriguez@qi.ub.es

^bInstitut de Nanociència i Nanotecnologia (IN²UB), Universitat de Barcelona, 08028 Barcelona, Spain

^cDepartament de Química, Universitat de les Illes Balears, 07071 Palma de Mallorca, Spain

^dLAQV-REQUIMTE, Departamento de Química, CQFB, Universidade Nova de Lisboa, Monte de Caparica, Portugal

† Electronic supplementary information (ESI) available. See DOI: <https://doi.org/10.1039/d2qi01267g>

In this context, we have designed gold(I) complexes containing a pyridyl type ligand with a PEG moiety incorporated into their chemical structure. Pyridyl type ligands are widely used in coordination chemistry due to their coordination ability properties. The number of gold(I) complexes with gold(I)-pyridyl bonds is lower than those with other ligands, such as gold(I)-phosphanes, due to the lower strength of the Au–N bond, but they deserve to be investigated.^{16–19} The second coordination position of the designed complexes contains a chromophore in order to introduce luminescence properties to the resulting systems. In-depth analysis of their aggregation and luminescence has been conducted. We are convinced that the formation of aggregates from the self-assembly of individual molecules deserves a careful analysis. The understanding of this phenomenon may open a number of possibilities and applications that deserve to be explored since the aggregates reported herein are stable in aqueous media.

Results and discussion

Synthesis and characterization

The synthetic route to gold(I) complexes involves different steps. Firstly, we synthesized the *N*-(4-pyridyl)-2-[2-(2-methoxyethoxy)ethoxy] acetic acid amide ligand (**1**) following the description reported in the literature.¹⁴

The introduction of gold(I) was carried out by the reaction of the common [AuCl(tht)] gold(I) precursor with **1** in order to obtain complex **2**. Its successful formation was proved by ¹H NMR, where a variation in the chemical shift was observed in the aromatic region (0.1 ppm upfield for H_a and 0.3 ppm downfield for H_b) and a 0.6 ppm downfield shift for NH protons (see Fig. S1†). Finally, alkynyl derivatives, 4-ethynylaniline (**L1**) or 7-propargylcoumarin (**L2**), were deprotonated with a strong base and then complex **2** was added in order to form the desired products **3** and **4** (Scheme 1).

The ¹H NMR spectra confirm the correct formation of the complexes due to the disappearance of the terminal alkynyl proton and a slight downfield shift (0.04 ppm) of the pyridyl protons close to the gold(I) atom together with the presence of the PEG protons (Fig. 1, S1 and S2†). It was also confirmed by ESI-MS(+) with the detection of the monoprotonated [M + H]⁺ species in both cases. The very small peaks detected in the ¹H NMR spectra (Fig. 1) can be ascribed to the initial formation of some aggregates that have been observed to be stable in DMSO (see the Theoretical calculations section below) and not to small impurities (the chemical shifts do not correspond to the starting reactants).

Photophysical characterization

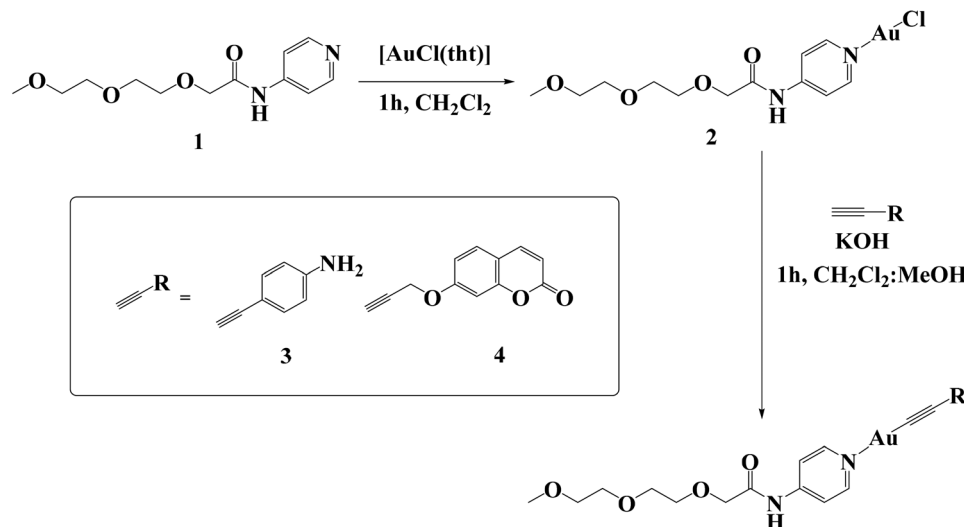
The absorption and emission spectra of all complexes have been recorded in 10^{−5} M acetonitrile solutions at room temperature and the obtained data are summarized in Table 1.

The absorption spectra of gold(I) complexes **3** and **4** display two absorption bands: one at higher energies (*ca.* 230 nm) related to the π–π* transition located in the pyridine ring and another at lower energies (*ca.* 300 nm) due to the π–π* transition of the alkynyl derivatives, 4-ethynylaniline (**L1**) or 7-propargylcoumarin (**L2**) (Fig. 2).^{20,21} The band at lower energies in both gold(I) complexes is slightly red shifted when gold(I) is coordinated to the chemical structure as observed in other similar compounds.^{20,22,23}

Emission spectra were recorded in solution upon excitation of the samples at the lowest energy absorption band. Ligand-centred fluorescence emission has been observed in **L1**, **L2** and their gold(I) derivatives with a slight red shift in the emission maxima.^{20,21} No emission was recorded for **1** and **2**.

Aggregation studies

The gold(I) complexes **3** and **4** contain a hydrophobic chromophore and a hydrophilic triethylene glycol pendant group that



Scheme 1 Synthetic route followed for the synthesis of complexes **3** and **4**.

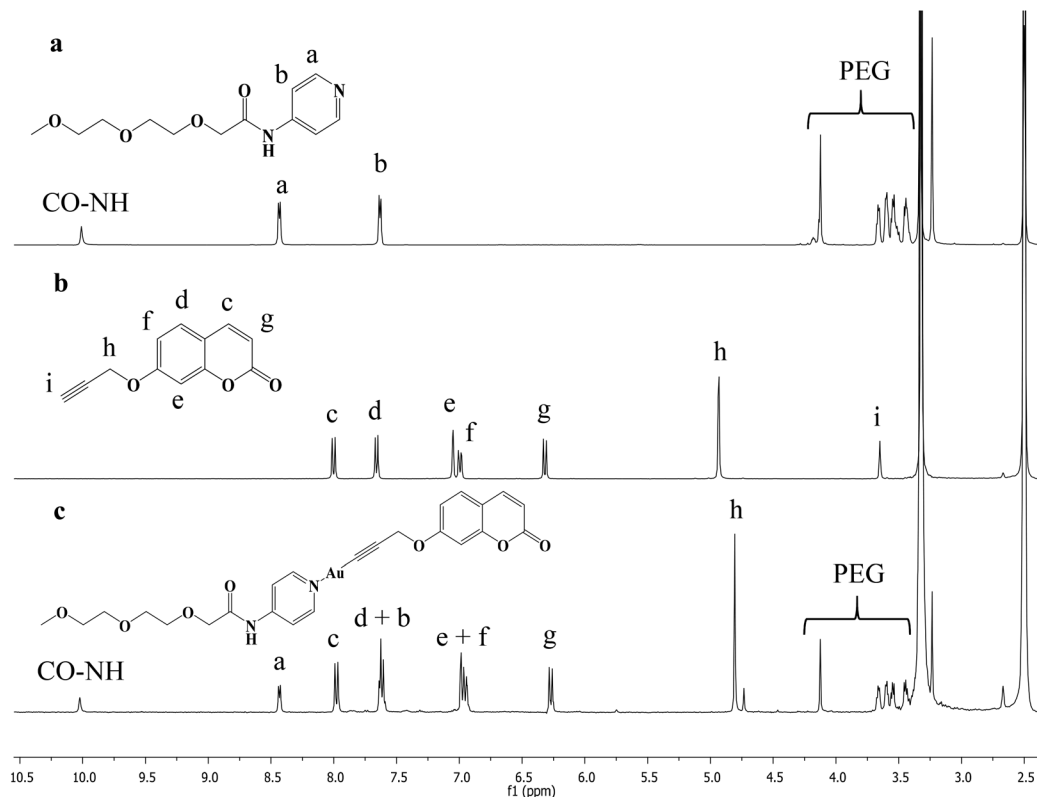


Fig. 1 ^1H NMR of **1** (a), 7-propargylcoumarin (b) and **4** (c) in DMSO-d_6 .

Table 1 Electronic absorption and emission data ($\lambda_{\text{exc}} = 280$ nm for **L1** and **3** and $\lambda_{\text{exc}} = 320$ nm for **L2** and **4**) of **1**, **L1** and **L2** and complexes **3** and **4** in acetonitrile

Compound	Absorption, nm λ_{max} ($10^3 \epsilon \text{ cm}^{-1} \text{ M}^{-1}$)	Emission λ_{max} (nm)
1	240 (16.6)	—
L1	273 (7.9)	346
L2	316 (16.0)	381
3	235 (11.1), 288 (19)	348
4	237 (16.5), 322 (18.0)	386

are expected to induce aggregation in water. In addition, the presence of an amide group, capable of favouring the establishment of additional directional hydrogen bonds, may play an important role in the resulting self-assembly process.

Studies of the variations of the luminescence properties of the complexes in solvent/non-solvent mixtures (acetonitrile/water, from 25% to 75% water content) have been performed in order to detect the existence of their expected aggregation. Acetonitrile has been used instead of DMSO due to the ideal cut-off of the solvent to record full absorption spectra. On the

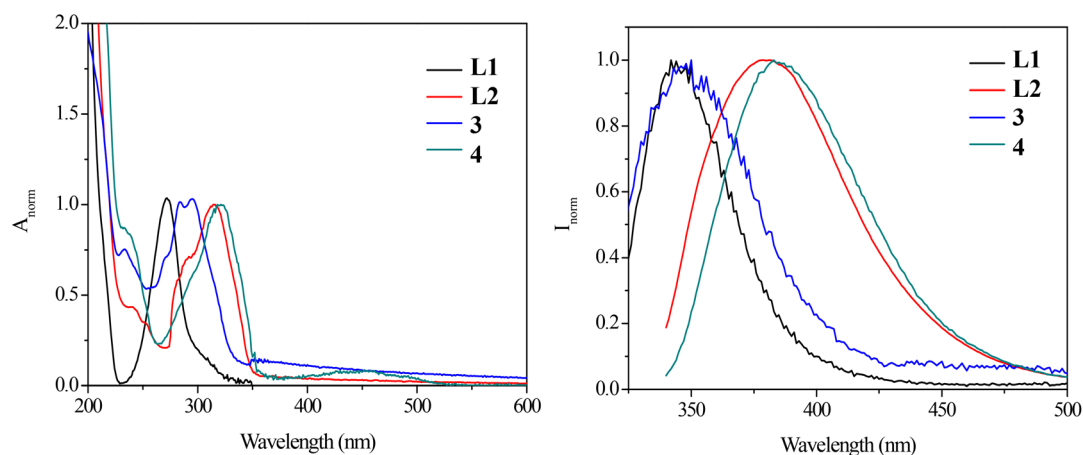


Fig. 2 Absorption (left) and emission (right) spectra of **L1** and **L2** and gold(I) complexes **3** and **4** in acetonitrile.

other hand, NMR studies could not be performed using acetonitrile due to solubility reasons. Nevertheless, the formation of comparable aggregation motifs is expected taking into consideration the similar polarity of both solvents (see the Theoretical calculations section below), although, of course, small differences in size and shape cannot be neglected.

Similar experiments were carried out with four other synthesized gold(I) complexes (5–8 in Fig. 3) containing PTA and DAPTA phosphanes instead of the pyridyl PEG ligand **1** and the same chromophore for comparison purposes in order to analyse the key role of **1** in the resulting aggregation. These complexes were previously synthesized by our group and we followed in this work the same synthetic procedure reported elsewhere.^{20,21}

Absorption and emission spectra were recorded for 3–8 at different water contents (25% to 75%). A blue shift (10 nm) is observed for compounds 3, 5 and 6 that contain 4-ethynylaniline as a chromophore (Fig. S3 and S4†). In the case of 3 the absorption band is the same as the **L1** absorption when the water content reaches 75%. This is probably due to the instability of the compound in the presence of water due to

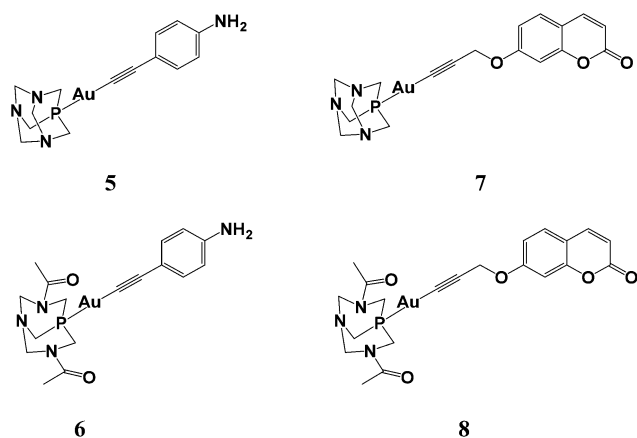


Fig. 3 Gold(I) complexes synthesized to analyse the role of **1** in the aggregation process.

the more labile character of the pyridyl–Au bond. No significant change in the absorption spectra was observed for those compounds containing 7-propargylcoumarin as a chromophore and PTA (**7**) or DAPTA (**8**) as a phosphane (Fig. S5 and S6†). In contrast, the incorporation of a hydrophilic PEG moiety (**4**) decreases the absorption band and increases the baseline in agreement with the aggregation process (Fig. 4, left).⁹ The recorded emission intensity of **4**, **7** and **8** increases at higher water contents, due to an aggregation induced emission (AIE) process (Fig. 4, S5 and S6†). Interestingly, a new emission band at a longer wavelength was detected in the case of **4**, when the water content was increased (Fig. 4). This band is attributed to the excimer of the coumarin unit, according to the literature.²⁴

Thus, the incorporation of the hydrophilic triethylene glycol pendant group at a second coordination position in the gold(I) complex that contains 7-propargylcoumarin (complex **4**) induces the formation of an excimer, meaning that the hydrophobic part of the molecules adopts conformations that minimize contact with water. Thus, we could expect the formation of a micellar or vesicle type aggregate, as exemplified in Fig. 5.

NMR studies in DMSO-*d*₆/D₂O mixtures were performed to obtain more information on the aggregation process. The ¹H NMR spectrum of **4** in pure DMSO-*d*₆ showed well-resolved signals with the correct integration, implying the major presence of discrete species (Fig. 6). A new set of signals were clearly observed in the region of the coumarin unit when water was added to the mixture (25%), suggesting the presence of two different types of species (monomer and aggregates or different types of aggregates) in solution where coumarin was directly involved.²²

Characterization of the aggregates

An in-depth characterization of the resulting aggregates in solution and in the solid state has been performed for gold(I) complex **4** in order to gain additional information on the size and shape of the resulting self-assembled structures. Dynamic light scattering (DLS) measurements showed the formation of aggregates in pure acetonitrile with a relatively narrow distri-

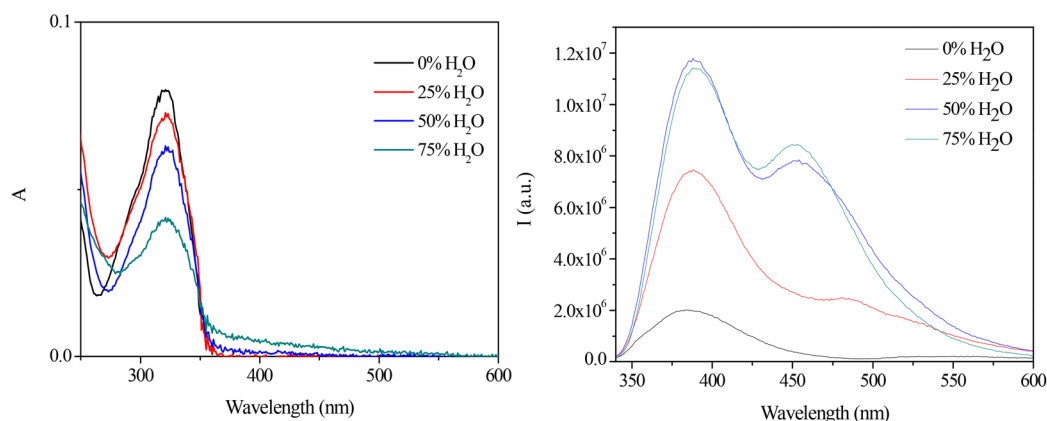


Fig. 4 Absorption (left) and emission (right) spectra of **4** in acetonitrile/water mixtures (10^{-5} M, 298 K).

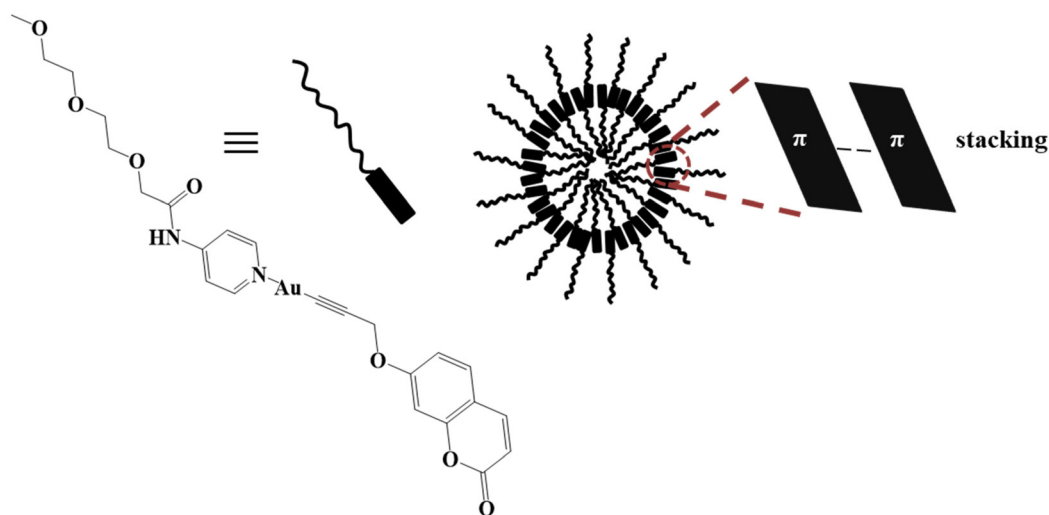


Fig. 5 Illustration of the supramolecular self-assembly expected for complex 4. Left, chemical formula and schematic representation of complex 4 and right, schematic illustration of the expected assembly.

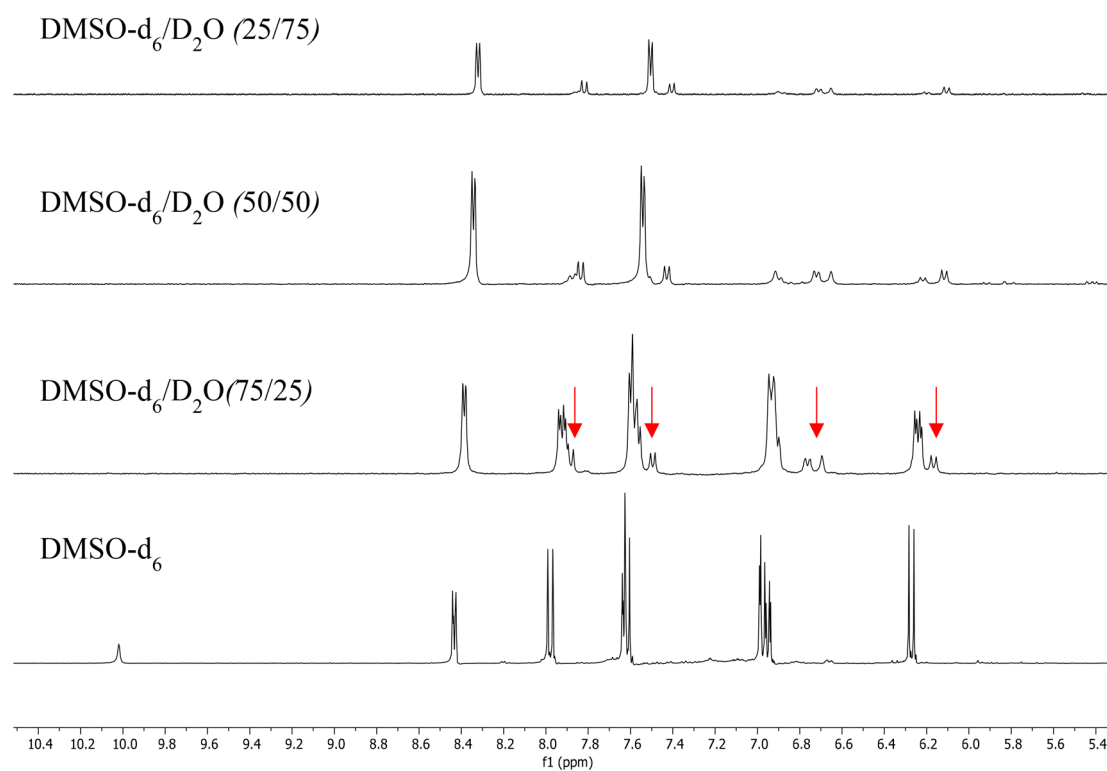


Fig. 6 ^1H NMR spectra of 4 in DMSO- $\text{d}_6/\text{D}_2\text{O}$ mixtures (10^{-4} M, 298 K).

bution (220 nm). Thus, aggregation already exists in the absence of water, in a good solvent such as acetonitrile, as previously observed in other gold(I) complexes.²⁶ The addition of different amounts of water induces an increase in the size of the aggregates being stabilized at *ca.* 400 nm (Fig. 7).

Small angle X-ray scattering (SAXS) studies were performed in order to analyze the size and the shape of the aggregates

during an early stage. The measurements were performed with 10^{-5} M solutions of gold(I) complex 4 dissolved in acetonitrile/water mixtures. The low-resolution structures were reconstructed *ab initio* from the scattering patterns using the DAMMIN program (Fig. 8).

The general tendency observed shows that the aggregates exist even in the very early stages, starting with very few mole-

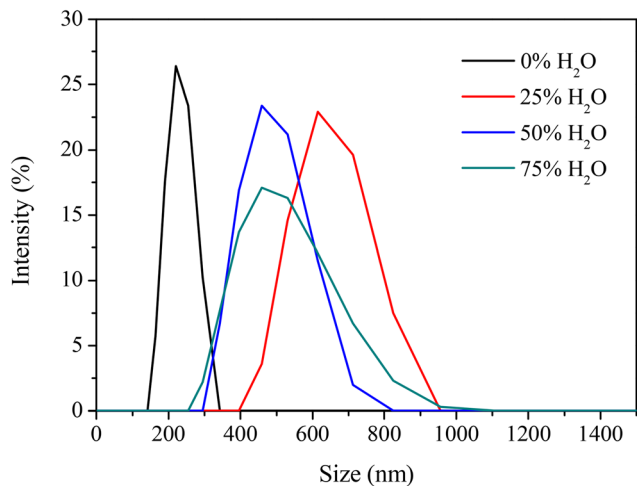


Fig. 7 Size distribution obtained by dynamic light scattering (DLS) of **4** at different water/acetonitrile ratios (10^{-5} M, 298 K).

cules in fresh acetonitrile solutions and then larger size structures result at higher water contents. These results agree with the data obtained in the DLS and photophysical experiments and confirm that the aggregation process is more favoured

when the water contents in the solvent mixture are increased. In this case, we can confirm the spherical package previously suggested (Fig. 5).

Optical microscopy (OM) also confirms this spherical aggregation motif. The samples were prepared by the deposition of solutions of gold(i) complex **4** with different acetonitrile/water mixtures onto a quartz substrate and allowing them to dry. The aggregates can be detected by optical microscopy when the water content reaches up to 50%, in agreement with more favoured aggregation. The optical microscopy images show the existence of spherical aggregates (A) and micrometric dendritic structures (B) (Fig. 9). It is expected that the more entangled supramolecular morphologies come from the interaction of the spherical aggregates as previously seen for gold(i) complexes.²⁵

The individual spherical aggregates of **4** of around 400 nm identified by DLS were also detected by scanning electron microscopy (SEM) (Fig. 10 and S7†). These spherical aggregates seemed to agglomerate to larger sizes as previously seen by OM (Fig. 9).

Cryo-transmission electron microscopy (cryo-TEM) was used to directly observe the supramolecular structure in the hydrated state. Until now the aggregates have been characterized by methods that require the evaporation of the solvent

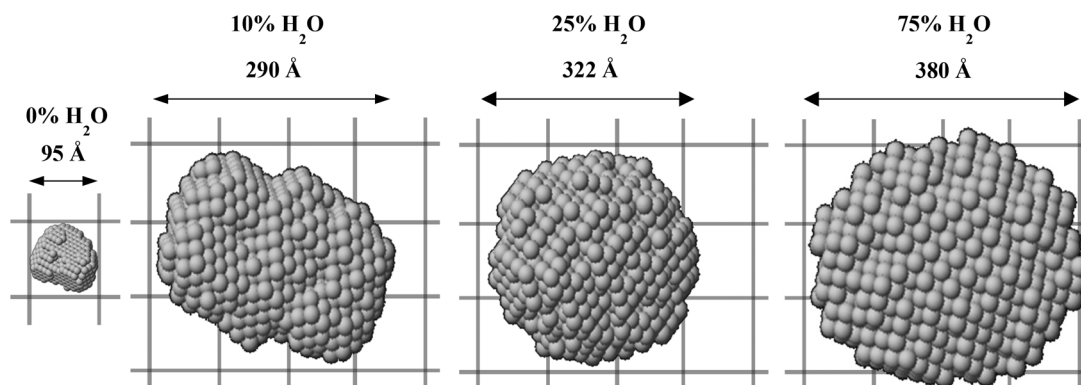


Fig. 8 DAMMIN low resolution structures reconstructed from SAXS patterns for **4** at different water/acetonitrile ratios (10^{-5} M, 298 K).

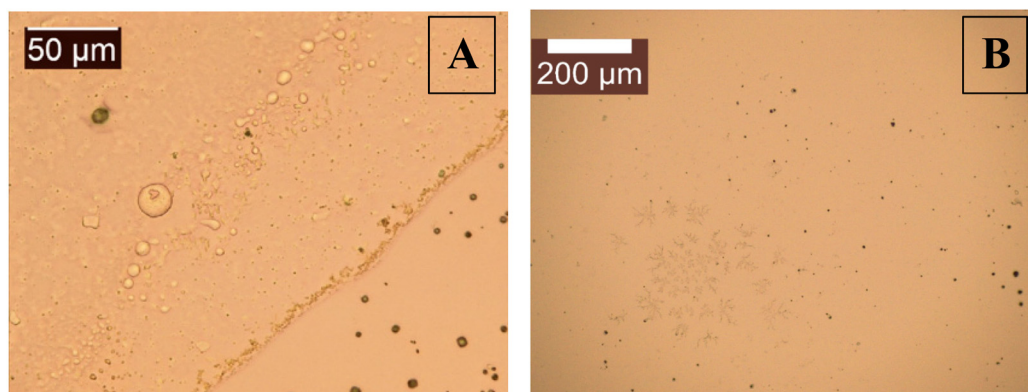


Fig. 9 Optical microscopy images of a dried solution of **4** in an acetonitrile/water mixture (25/75) (5×10^{-5} M, 298 K) showing the existence of spherical aggregates (A) and micrometric dendritic structures (B).

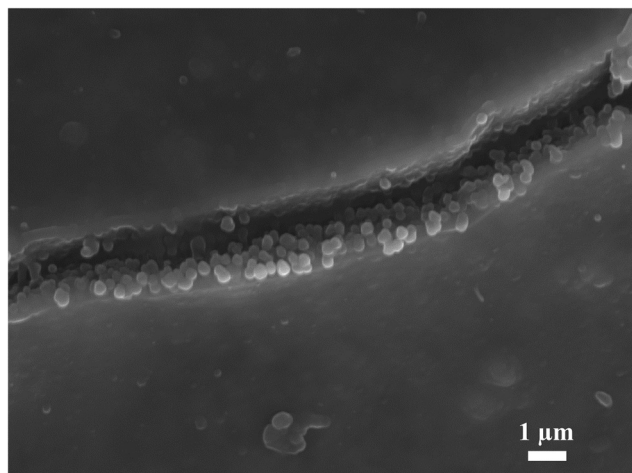


Fig. 10 SEM micrograph of **4** in an acetonitrile/water mixture (25/75) (5×10^{-5} M, 298 K).

that can cause changes in the composition or rearrangement of the sample or methods that use mathematical models.²⁶ In fact, cryo-TEM allows us to identify that the spherical aggregates observed previously present an empty inner cavity in solution (Fig. 11 and S8†). The very large size observed fits perfectly using the different microscopy techniques and aggregates can be either very large vesicles or some kind of conglomerate (acervates).

Analysis of the crystal packing parameter (CPP)

The morphology of the aggregates is determined by the critical packing parameter (CPP). The CPP itself depends on three structural parameters: (1) the volume of the hydrophobic block; (2) the area of a cross-section of the more hydrophilic part; and (3) the length of the hydrophobic part.¹¹ Calculation of the CPP value for complex **4** was carried out by measuring the length of the molecule based on an optimized Gaussian

model (Fig. 12). The calculated CPP value was 1, which agrees with the formation of a vesicle aggregate.²⁷

Calculation of the number of molecules involved in the vesicles (N_{agg})

An in-depth study of the size of the early stage (micellar) aggregates that later will merge into vesicles can be performed by the previous calculation of the aggregation number (N_{agg}) of the molecules that constitute these supramolecular assemblies. This parameter can be obtained by fluorescence techniques using a probe that can be included within the supramolecular assemblies and a quencher that will modify the photo-physical properties of the probe (emission intensity and lifetime). Pyrene and cetylpyridinium chloride (CPC) have been used as the probe and quencher, respectively, following a methodology previously described in the literature.²⁸

Thus, following the theory developed by Turro and Yekta^{29,30} the relationship between the emission intensity of a micellar-type structure in the presence (I) and in the absence (I_0) of a quencher was found to be directly affected by the concentration of the micelles $[M]$ and the quencher $[Q]$, according to the equation:

$$\ln(I_0/I) = Q/M, \quad (1)$$

where $M = (C - \text{CMC})/N_{\text{agg}}$, with C being the total surfactant concentration, CMC the critical micelle concentration and N_{agg} the aggregation number. Thus, the plot of $\ln(I_0/I)$ vs. Q will be directly correlated with the N_{agg} by the slope ($1/M$).

We then recorded the emission of our gold(i) aggregates in the presence of pyrene (as the probe) and different amounts of quencher (Fig. S9†). The emission spectra show the presence of two bands. The highest energy emission band is due to the presence of the pyrene (probe), which is directly affected by the addition of the quencher. The second band, at a longer wavelength, is a broad band at ca. 450 nm that corresponds to the band previously assigned to the π - π stacking of the cou-

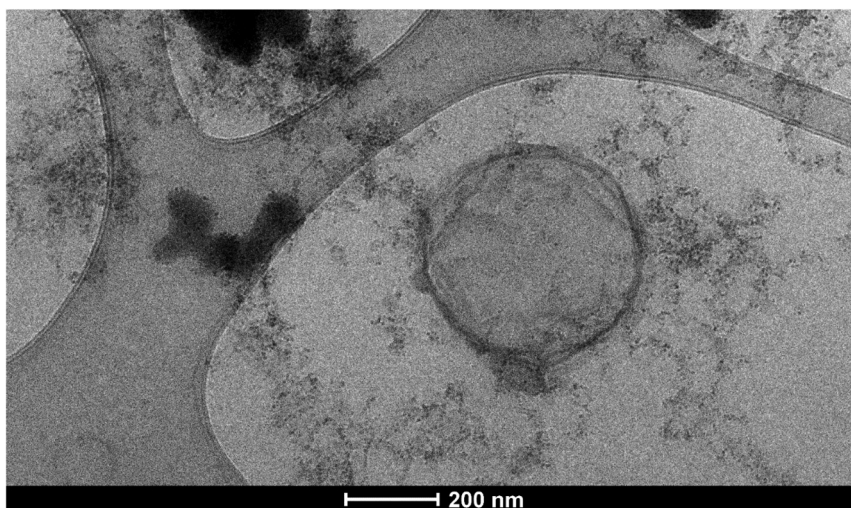


Fig. 11 Cryo-TEM micrograph of **4** in a DMSO/water mixture (25/75) (5×10^{-5} M, 103 K).

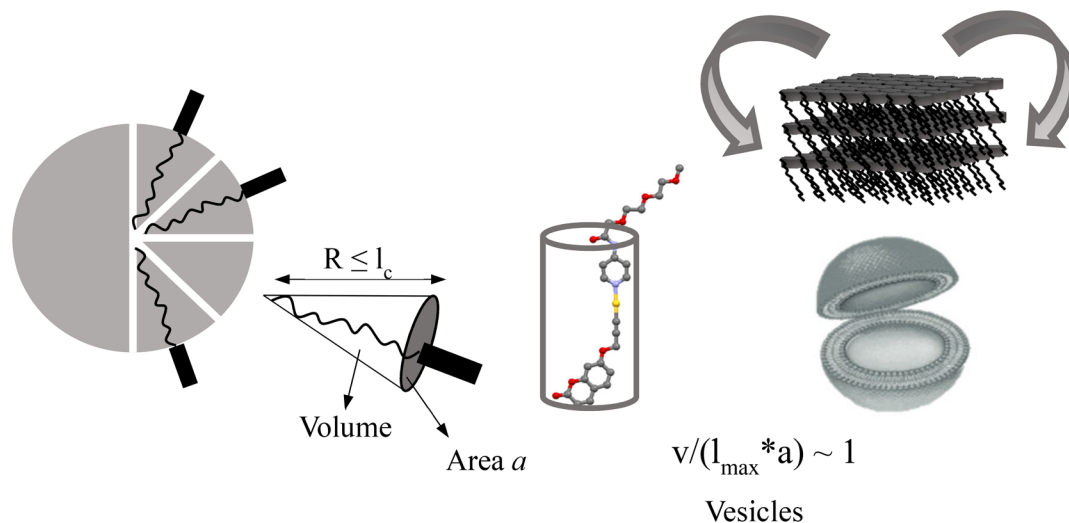


Fig. 12 Critical packing parameter (CPP) and the preferred aggregate structure for the geometrical packing of 4.

marin groups. Interestingly, this band is not affected by the presence of the quencher being just involved in the formation of the assemblies. From these data we could retrieve the N_{agg} number but, according to the literature, it is necessary to check firstly the $\tau_0 k_q$ product (with τ_0 being the lifetime of the pyrene in the absence of a quencher and k_q the first order intramicellar rate constant for quenching in a micelle with one quencher). To measure $\tau_0 k_q$, emission lifetimes were measured for pyrene quenching by CPC within the gold(i) micellar assemblies (see Fig. S10†). The simplest case will be to consider that the fluorescent probe and the quencher stay in or on a micelle for a time longer than the unquenched lifetime of the fluorophore. Assuming this, the fluorescence decay of the probe is given by the equation:

$$I(t) = A_0 \exp(-A_1 t - A_2(1 - \exp(-A_3 t))) \quad (2)$$

where A_0 is the intensity of the emission at time zero, A_1 is $1/\tau_0$, $A_2 = Q/M$ and $A_3 = k_q$.^{29–32}

The lifetimes of pyrene measured in the presence of gold(i) micellar-type aggregates, and with increasing amounts of quencher, present a parallel profile at longer times. This is the simplest situation for the mathematical treatment and indicates that the quencher is not moving freely between the micelles and the aqueous phase. A blank experiment was also carried out with only the probe and the quencher and a similar variation was recorded as an indication of the effective emission quenching of the pyrene by the selected CPC quencher. The recorded τ_0 value for pyrene is 152 ns, similar to other values reported previously in the literature for this type of experiment.^{28,33}

With this information, eqn (1) can be applied and, from there, the N_{agg} was calculated to be 82 ± 3 , which is a quite reasonable number for a micellar-aggregate.²⁷

Theoretical calculations

We have modeled a micelle composed of 70 units of compound 4 in water using theoretical calculations. For this purpose, we have used the extended semiempirical tight-binding model (GFN2-xTB) developed by Grimme *et al.*³⁴ This method was designed for the fast calculation of structures and noncovalent interaction energies for molecular systems with roughly 1000 atoms, although the micelle studied herein is composed of 3450 atoms. This model has been limited to 70 molecules in order to ensure the calculation is doable and provides a reasonable approximation to the experimental results. The novelty of the GFN2-xTB method is the inclusion of anisotropic second order density fluctuation effects. It results in a more physically sound method compared to standard semiempirical methods. Furthermore, the D4 dispersion model is incorporated self-consistently, allowing an adequate description of π -stacking interactions. This method is well-suited to explore the conformational space of molecular systems.³⁴

Fig. 13(a) shows the optimized geometry of the micelle exhibiting a spherical shape with a diameter that ranges from 85 to 90 Å. This value agrees with the data recorded by SAXS experiments in the absence of water. Keeping in mind that this structure is simply one minimum among the many other possible minima that most likely exist in the potential hypersurface (highly dynamic system), the size of the micelle is expected to be similar for all minima. Moreover, since the micelle is composed of a significant number of molecules, it is useful to examine the different types of interactions the coumarin ring establishes in the aggregate. They are expected to be similar in all the possible geometric minima of the micelle. We have observed that the coumarin ring mostly participates in π -stacking interactions, in line with the experimentally observed photophysical properties of the aggregates. We have basically observed two different binding modes that have been

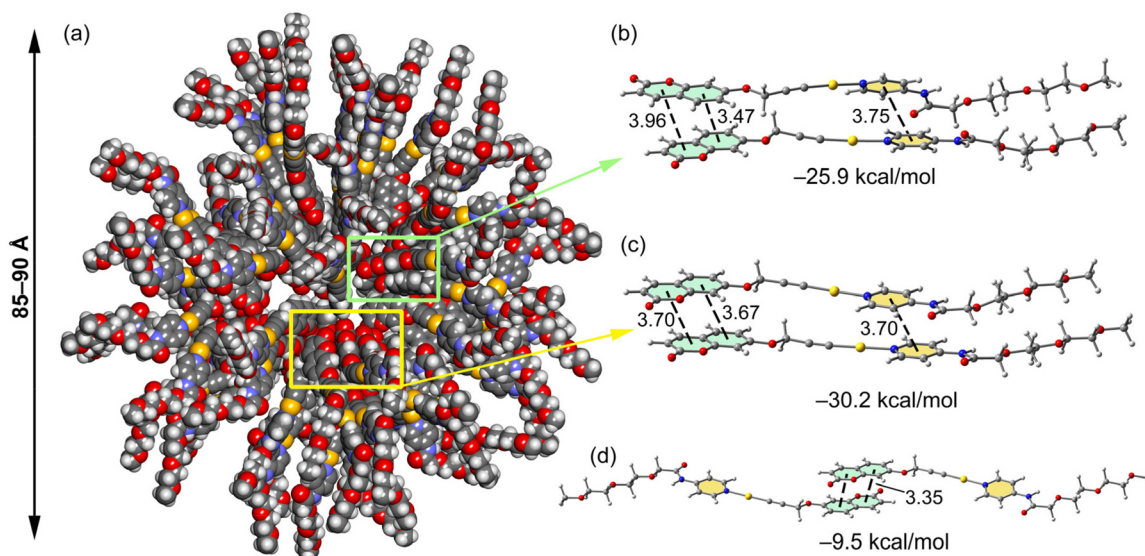


Fig. 13 (a) Optimized geometry of the micelle composed of 70 molecules of compound **4** at the GFN2-xTB level of theory. (b)–(d) RI-BP86-D3/def2-TZVP optimized geometries of three π -stacked dimers of **4**. Distances in Å, measured between the ring centroids.

further evaluated using DFT calculations in water. Moreover, a third binding mode, not observed experimentally, has also been evaluated and compared with the other two π -stacking binding modes. These calculations have been performed taking into consideration water as the solvent at the RI-PB86-D3(COSMO)/def2-TZVP level of theory. The results are summarized in Fig. 13(b) and (c), where the optimized geometries, π -stacking distances and binding energies are provided. It can be observed that the parallel displaced orientation (Fig. 13(c)) is slightly more favored than the binding mode where one of the coumarin rings is rotated 180° with respect to the other one (Fig. 13(b)). In both π -stacking modes the Au-coordinated pyridine rings also establish a parallel displaced π -stacking interaction with similar distances. A third binding mode (anti-parallel π -stacking) was also evaluated, showing the weakest interaction ($-9.5 \text{ kcal mol}^{-1}$) due to the absence of the additional π -stacking interaction between the pyridine rings and the additional van der Waals forces due to the PEG chains and triple bonds (Fig. 13(d)).

Since some of the experiments have been performed in mixtures of DMSO/water (NMR) and others in mixtures of acetonitrile/water (photophysical characterization) for technical reasons, and we have compared the energies and geometries of the representative π -stacked assemblies in both solvents (dimers in Fig. 13(b) and (c)). Gratifyingly, we obtained almost identical dimerization energies and equilibrium distances (see ESI, Fig. S11†) as expected taking into account the similar polarity of the solvents, further supporting a similar aggregation.

Taking all of this into consideration, we can postulate that our gold(I) complex produces micelles in solution with a size of around 90 \AA that are constituted by around 80 molecules. These micelles will form larger coacervated aggregates, assuming a double layer lamellar phase with water inside and

outside the vesicles, where the PEG tail will face water and the coumarin ring will be protected from water, as identified by the different microscopy techniques and DLS.

Thermodynamic data that govern the assemblies

In an attempt to obtain thermodynamic information from the self-assembly process of gold(I) complex **4**, ^1H NMR experiments at different temperatures were performed. The increase of the temperature gives rise to an increase of the second set of signals attributed to the aggregates (Fig. 14). The recorded variations of the peak intensities follow a sigmoidal behavior that fits with an isodesmic model. In this assumption, all the constants are considered equal and the following equation can be applied:

$$c_0 = \frac{c_1}{(1 - c_1K)^2} \quad (3)$$

where c_1 is the concentration of the monomer, c_0 is the total concentration and K is the aggregation constant.

By transforming in terms of molar fractions eqn (3) becomes:

$$\text{Monomer : } x_1 = \frac{c_1}{c_0} = \frac{1 + 2Kc_0 - \sqrt{1 + 4Kc_0}}{2K^2c_0^2} \quad (4)$$

$$\text{Aggregates : } x_n = 1 - x_1 = 1 - \frac{1 + 2Kc_0 - \sqrt{1 + 4Kc_0}}{2K^2c_0^2} \quad (5)$$

The values obtained from the fittings and the application of eqn (6) are summarized in Table 2:

$$K = e^{-(\Delta H/RT) + (\Delta S/R)}. \quad (6)$$

These data show that the aggregation of **4** is endothermic at least in the temperature range studied. This means that this

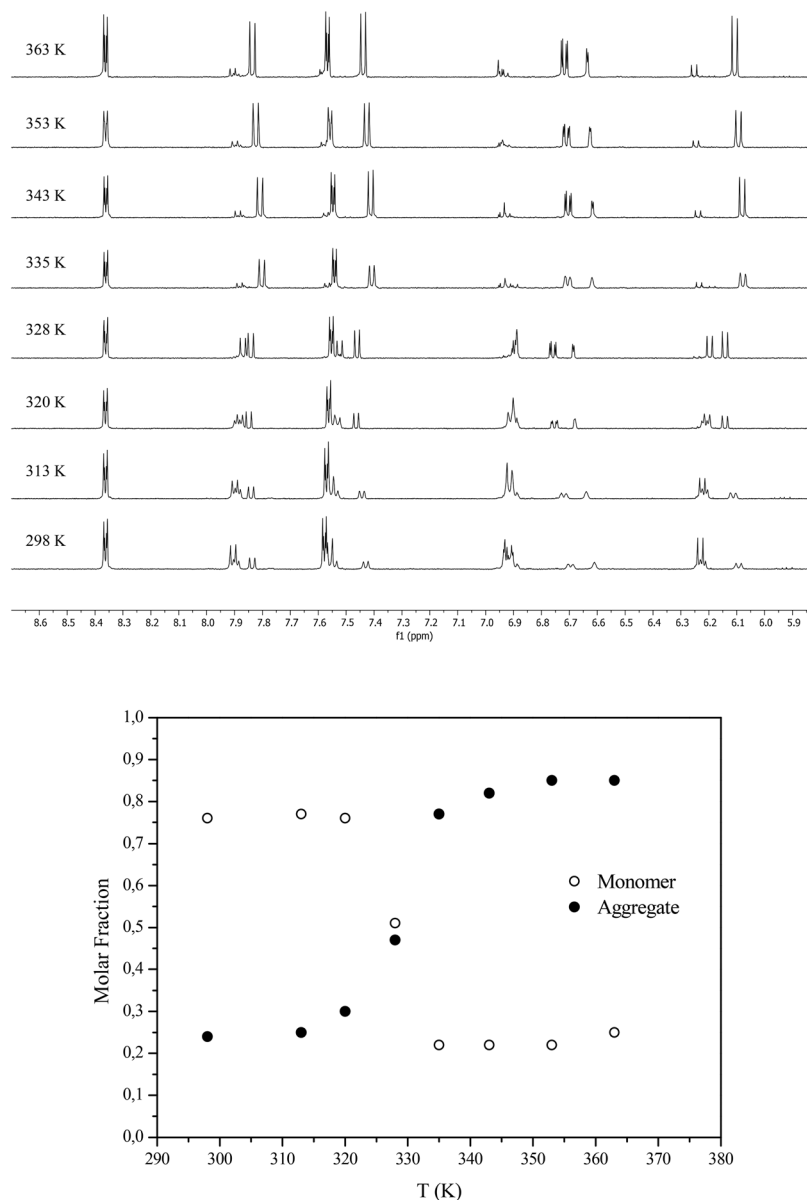


Fig. 14 (above) ¹H NMR spectra of the 4×10^{-3} M DMSO-*d*₆/D₂O mixture (75/25) of **4** at different temperatures (10^{-4} M); (below) open circles – molar fraction of the monomer; closed circles – molar fraction of aggregates.

Table 2 Enthalpy (ΔH), entropy (ΔS), free energy (ΔG) at 298 K, and aggregation constant (K) at 298 K for the DMSO/water mixture of compound **4**

Compound	$\Delta H/\text{kJ mol}^{-1}$	$\Delta S/\text{J mol}^{-1} \text{K}^{-1}$	$\Delta G^{298}/\text{kJ mol}^{-1}$	K^{298}
4	82	294	-5	41

process is not driven by enthalpic factors, such as in the stabilizing interactions (H-bonds or π - π stacking) but by entropic factors. We attributed this behavior to the exclusion of water molecules, as the release of ordered solvent molecules from the PEG side chains increases the entropy of the system and the aggregation process is still energetically favorable. This

entropically driven molecular assembly was previously observed with other systems containing an amphiphilic moiety.^{35–37}

Conclusions

The presence of a polyethyleneglycol pendant unit in a gold(I) compound induces the formation of vesicles, as supported by the calculation of the CPP. These vesicles aggregate forming larger coacervates that are observed under a microscope (optical and electron). The use of cryo-TEM supports the observation of empty inner cavities in the resulting aggregates.

Emission spectra were decisive in the analysis of the aggregates since: (i) they can determine the presence of π - π stacking between the chromophoric groups (coumarins), as supported also by DFT calculations; (ii) we have been able to determine the number of molecules forming the early stage micellar aggregates that later merge into the observed vesicles thanks to an in-depth analysis of the quenching process of a probe within the vesicles.

NMR experiments recorded spectra at different temperatures that allowed us to confirm that entropy is the driving force for the formation of these vesicular-type assemblies.

The analysis of these types of aggregates opens new possibilities for applications in the supramolecular chemistry field and even more within green chemistry since the aggregates are stable in aqueous media.

Experimental section

General procedures

All manipulations have been performed under prepurified N_2 using standard Schlenk techniques. All solvents have been distilled from appropriate drying agents. Commercial reagents 4-aminopyridine (Aldrich, 98%), *N,N'*-dicyclohexylcarbodiimide (Aldrich, 99%), 2-[2-(2-methoxyethoxy)ethoxy]acetic acid (Aldrich), 4-ethynylaniline (Aldrich, 97%), propargyl bromide (Aldrich, 80 wt% toluene), and 7-hydroxy-1-benzopyran-2-one (Aldrich) were used as received. Literature methods were used to prepare *N*-(4-pyridyl)-2-[2-(2-methoxyethoxy)ethoxy]acetic acid amide (**1**)^{14,15} and 7-(prop-2-in-1-yloxy)-1-benzopyran-2-one.³⁸

Physical measurements

Infrared spectra were recorded on a FT-IR 520 Nicolet spectrophotometer. ¹H-NMR (δ (TMS) = 0.0 ppm) and ³¹P{¹H}-NMR (δ (85% H_3PO_4) = 0.0 ppm) spectra were obtained on Varian Mercury 400 and Bruker 400 spectrometers, respectively (Universitat de Barcelona). Electrospray-mass spectra (+) were recorded on a Fisons VG Quatro spectrometer (Universitat de Barcelona). Absorption spectra were recorded on a Varian Cary 100 Bio UV-spectrophotometer and emission spectra on a Horiba-Jobin-Yvon SPEX Nanolog spectrofluorimeter (Universitat de Barcelona). Dynamic light scattering (DLS) measurements were carried out on a Zetasizer NanoS spectrometer (Universitat de Barcelona). The samples were measured in quartz cuvettes. SAXS experiments were performed on the NCD-SWEET beamline at the ALBA Synchrotron at 12.4 keV, and the sample/detector distance was 6.2 m to cover the range of momentum transfer of $0.028 < q < 2.56 \text{ nm}^{-1}$. The data were collected on a Pilatus3S 1M detector with a pixel size of $172.0 \times 172.0 \mu\text{m}^2$. The exposure time was 30 s. The *q*-axis calibration was obtained by measuring silver behenate.³⁹ The pyFAI program was used to integrate the 2D SAXS data into 1D data.⁴⁰ The data were then subtracted from the background using PRIMUS software.⁴¹ The maximum particle dimension, D_{max} , and the pair distance distribution, $P(r)$, were determined

with GNOM.⁴² The low resolution structure of aggregates was reconstructed *ab initio* from the initial portions of the scattering patterns using the DAMM program.⁴³ Optical microscopy images were acquired on a Leica ICC50 W microscope equipped with a Nikon DXM1200F digital camera. Scanning electron microscopy (SEM) was carried out at 20 kV using a J-7100F (Jeol) equipped with a thermal field electron source. Cryo-transmission electron microscopy measurements were carried out with a Tecnai G2 F20 (FEI) 200 kV FEG TEM cryomicroscope.

Theoretical methods

The initial optimization of the micellar aggregates was performed using the semiempirical tight-binding (GFN2-xTB) method³⁴ and the xTB program developed by Grimme and co-workers.⁴⁴ Solvent effects have been included with the GBSA model, which combines the generalized Born (GB) model for electrostatic solvation effects and a solvent accessible surface area (SA) term for nonpolar contributions.

All density functional theory calculations were carried out with the TURBOMOLE 7.0 software package.⁴⁵ DFT-optimizations were performed using the cost-effective BP86^{46,47}-D3⁴⁸ functional, which combined Grimme's D3 approximation⁴⁸ with the Becke-Johnson function,⁴⁹ and the triple- ζ def2-TZVP basis set.⁵⁰ For gold, the inner shell electrons were modelled by ECPs (ECP-60 scheme),⁵¹ which also accounted for scalar relativistic effects. Solvent effects were taken into consideration using the conductor-like solvation model (COSMO)⁵² as implemented in TURBOMOLE 7.0. The Cartesian coordinates of the optimized dimers are given in the ESI.†

Preparation of the samples

Preparation of the vesicles. Complex **4** was dissolved in mixtures of acetonitrile/water or DMSO/water using concentrations above 10^{-5} M in order to prepare the aggregates.

Optical microscopy measurements. A $5 \times 10^{-5} \text{ M}$ solution of complex **4** was dissolved in acetonitrile/water mixtures (25/75). For the measurement, a drop of the solution was placed onto a microscope slide and evaporated to dryness.

SEM measurements. A $5 \times 10^{-5} \text{ M}$ solution of complex **4** dissolved in acetonitrile/water mixtures (25/75) was prepared. A drop of the solution was deposited onto a silicon plate and evaporated to dryness by contact with air.

Synthesis and characterization

Synthesis of [AuCl(pyPEG)] (2). [AuCl(tht)] (0.1999 g, 0.6228 mmol) was dissolved in CH_2Cl_2 (5 mL) in a purged Schlenk flask protected with aluminium foil. pyPEG (0.1558 g, 0.6131 mmol) was dissolved in CH_2Cl_2 (5 mL). The pyPEG solution was added dropwise to the [AuCl(tht)] solution under stirring, resulting in a white suspension. After 1 h of stirring, the reaction mixture was concentrated in a vacuum to half the volume and hexane (5 mL) was then added in order to favour precipitation. The resulting white solid was filtered and dried under vacuum. Yield: 69% (0.1285 g).

^1H NMR (CDCl_3 , ppm): 9.53 (br. s, 1H, N-H), 8.40 (d, $J = 6.0$ Hz, 2H, $\text{N}_{\text{py}}\text{-CH}$), 7.89 (d, $J = 6.0$ Hz, 2H, $\text{N}_{\text{py}}\text{-CH-CH}$), 4.15 (s, 2H, CO-CH_2), 3.60–3.78 (m, 8H, $\text{CH}_3\text{-O-CH}_2\text{-CH}_2\text{-O-CH}_2\text{-CH}_2$), 3.38 (s, 3H, $-\text{CH}_3$). IR (KBr, cm^{-1}): $\nu(\text{N-H})$: 3452, $\nu(\text{C=O})$: 1714, $\nu(\text{C=N})$: 1622. ESI-MS (+) m/z : 487.0596 ($[\text{M} + \text{H}]^+$, calc.: 487.0694).

Synthesis of [Au(4-ethynylaniline)(pyPEG)] (3). 4-Ethynylaniline (0.0148 g, 0.1263 mmol) was reacted with KOH (0.0196 g, 0.3493 mmol) in MeOH (5 mL) under a N_2 atmosphere. $[\text{AuCl}(\text{pyPEG})]$ (0.0596 g, 0.1225 mmol) was dissolved in CH_2Cl_2 (5 mL) and this solution was added dropwise to the previous one, leading to the formation of a reddish brown solid. After 1 h of stirring, the reaction mixture was concentrated under vacuum to half the volume and hexane (5 mL) was then added in order to favour precipitation. The resulting reddish solid was filtered and dried under vacuum. Yield: 59% (0.0410 g).

^1H NMR ($\text{acn-}d_3$, ppm): 9.03 (br. s, 1H, N-H), 8.45 (d, $J = 6.0$ Hz, 2H, $\text{N}_{\text{py}}\text{-CH}$), 7.61 (d, $J = 6.0$ Hz, 2H, $\text{N}_{\text{py}}\text{-CH-CH}$), 7.00 (d, $J = 8.2$ Hz, 2H, H_β), 6.49 (d, $J = 8.2$ Hz, 2H, H_α), 3.30 (s, 3H, $-\text{CH}_3$), 4.07 (s, 2H, $-\text{NH}_2$), 4.05 (s, 2H, CO-CH_2), 3.48–3.75 (m, 8H, $\text{CH}_3\text{-O-CH}_2\text{-CH}_2\text{-O-CH}_2\text{-CH}_2$). IR (KBr, cm^{-1}): $\nu(\text{N-H})$: 3436, $\nu(\text{C}\equiv\text{C})$: 1996, $\nu(\text{C=O})$: 1715, $\nu(\text{C=N})$: 1619. ESI-MS (+) m/z : 568.1496 ($[\text{M} + \text{H}]^+$, calc.: 568.1505).

Synthesis of [Au(7-propargylcoumarin)(pyPEG)] (4). 7-Propargylcoumarin (0.0184 g, 0.0919 mmol) was treated with KOH (0.0112 g, 0.1996 mmol) in MeOH (5 mL) under a N_2 atmosphere. $[\text{AuCl}(\text{pyPEG})]$ (0.0447 g, 0.0918 mmol) was dissolved in CH_2Cl_2 (5 mL) and this solution was added dropwise to the previous one, leading to the formation of an ochre solid. After 1 h of stirring, the reaction mixture was concentrated under vacuum to half the volume and hexane (5 mL) was then added in order to favour precipitation. The resulting pale brown solid was filtered and dried under vacuum. Yield: 63% (0.0310 g).

^1H NMR ($\text{DMSO-}d_6$, ppm): 10.03 (br. s, 1H, N-H), 8.44 (d, $J = 6.0$ Hz, 2H, $\text{N}_{\text{py}}\text{-CH}$), 7.99 (d, $J = 9.5$ Hz, O-CO-CH-CH), 7.64 (d, $J = 6.0$ Hz, 2H, $\text{N}_{\text{py}}\text{-CH-CH}$), 7.61 (d, $J = 8.5$ Hz, 1H, O-CO-CH-CH-C-CH), 6.29 (d, $J = 9.5$ Hz, 1H, O-CO-CH), 7.00–6.94 (m, 2H, $\text{CH}_2\text{-O-C-CH}$), 3.24 (s, 3H, $-\text{CH}_3$), 4.81 (s, 2H, $\text{C}\equiv\text{C-CH}_2$), 4.13 (s, 2H, $-\text{NH}_2$), 3.42–3.68 (m, 8H, $\text{CH}_3\text{-O-CH}_2\text{-CH}_2\text{-O-CH}_2\text{-CH}_2$). IR (KBr, cm^{-1}): $\nu(\text{N-H})$: 3436, $\nu(\text{C}\equiv\text{C})$: 2135, $\nu(\text{C=O})$: 1720, $\nu(\text{C=N})$: 1612. HRESI-MS (+) m/z : 651.1409 ($[\text{M} + \text{H}]^+$, calc.: 651.1400).

Author contributions

Dr Andrea Pinto: investigation, methodology, data curation, formal analysis, and writing the original draft; Jaume Sonet: investigation; Dr Rosa M. Gomila: investigation; Prof. Antonio Frontera: investigation, supervision, and writing – review and editing; Prof. João Carlos Lima: investigation, supervision, and validation; Prof. Laura Rodríguez: supervision, writing, review and editing, resources, conceptualization, and project administration.

Conflicts of interest

There are no conflicts to declare.

Acknowledgements

The authors are grateful to the Ministerio de Ciencia e Innovación of Spain (Projects PID2019-104121GB-I00 and PID2020-115637GB-I00). This work was supported by the Associate Laboratory for Green Chemistry-LAQV, which is financed by national funds from FCT/MCTES (UID/QUI/50006/2019). The authors would also like to acknowledge the International Research Network Hetero-elements and Coordination Chemistry: from Concepts to Applications (HC3A) and Spanish Network Materiales Supramoleculares Funcionales (RED2018-102331-T). This article is based on work from COST Actions CA 17140 “Cancer Nanomedicine from the Bench to the Bedside” and CA18202—NECTAR supported by COST (European Cooperation in Science and Technology). SAXS experiments were performed at the NCD-BL11 beamline of the ALBA Synchrotron Light Facility in collaboration with the ALBA staff.

References

- 1 M. de Loos, B. L. Feringa and J. H. van Esch, Design and Application of Self-Assembled Low Molecular Weight Hydrogens, *Eur. J. Org. Chem.*, 2005, 3615–3631.
- 2 M. McCullagh, T. Prytkova, S. Tonzani, N. D. Winter and G. C. Schatz, Modeling Self-Assembled Processes Driven by Nonbonded Interactions in Soft Materials, *J. Phys. Chem. B*, 2008, **112**, 10388–10398.
- 3 X. Zhuang, Y. Mai, D. Wu, F. Zhang and X. Feng, Two-Dimensional Soft Nanomaterials: A Fascinating World of Materials, *Adv. Mater.*, 2015, **27**, 403–427.
- 4 J. M. Lehn, From supramolecular chemistry towards constitutional dynamic chemistry and adaptive chemistry, *Chem. Soc. Rev.*, 2007, **36**, 151–160.
- 5 X. Yan, F. Wang, B. Zheng and F. Huang, Stimuli-responsive supramolecular polymeric materials, *Chem. Soc. Rev.*, 2012, **41**, 6042–6065.
- 6 J. Wang, Z. Huang, X. Ma and H. Tian, Visible-Light-Excited Room-Temperature Phosphorescence in Water by Cucurbit[8]uril-Mediated Supramolecular Assembly, *Angew. Chem., Int. Ed.*, 2020, **59**, 9928–9933.
- 7 H. Schmidbaur and A. Schier, Auophilic interactions as a subject of current research: an up-date, *Chem. Soc. Rev.*, 2012, **41**, 370–412.
- 8 J. C. Lima and L. Rodríguez, Application of gold(i) alkynyl systems: a growing field to explore, *Chem. Soc. Rev.*, 2011, **40**, 5442–5456.
- 9 A. Pinto, N. Svahn, J. C. Lima and L. Rodríguez, Aggregation induced emission of gold(i) complexes in

- water or water mixtures, *Dalton Trans.*, 2017, **46**, 11125–11139.
- 10 E. Aguiló, R. Gavara, J. C. Lima, J. Llorca and L. Rodríguez, From Au(i) organometallic hydrogels to well-defined Au(0) nanoparticles, *J. Mater. Chem. C*, 2013, **1**, 5538–5547.
 - 11 E. Aguiló, R. Gavara, C. Baucells, M. Guitart, J. C. Lima, J. Llorca and L. Rodríguez, Tuning supramolecular aurophilic structures: the effect of counterion, positive charge and solvent, *Dalton Trans.*, 2016, **45**, 7328–7339.
 - 12 R. Gavara, E. Aguiló, J. Schur, J. Llorca, I. Ott and L. Rodríguez, Study of the effect of the chromophore and nuclearity on the aggregation and potential biological activity of gold(i) alkynyl complexes, *Inorg. Chim. Acta*, 2016, **446**, 189–197.
 - 13 F. Schroeter, J. Soellner and T. Strassner, Cyclometalated palladium NHC complexes bearing PEG chains for Suzuki-Miyaura cross-coupling in water, *Organometallics*, 2018, **37**, 4267–4275.
 - 14 A. Aliprandi, M. Mauro and L. De Cola, Controlling and imaging biomimetic self-assembly, *Nat. Chem.*, 2016, **8**, 10–15.
 - 15 S. Carrara, A. Aliprandi, C. F. Hogan and L. De Cola, Aggregation-induced electrochemiluminescence of platinum(II) complexes, *J. Am. Chem. Soc.*, 2017, **139**, 14605–14610.
 - 16 Z. Chen, G. Liu, S. Pu and S. H. Liu, Bipyridine-based aggregation-induced phosphorescent emission (AIPE)-active gold(i) complex with reversible phosphorescent mechanochromism and self-assembly characteristics, *Dyes Pigm.*, 2018, **152**, 54–59.
 - 17 J. J. González, E. Ortega, M. Rothmund, M. Gold, C. Vicente, C. de Haro, D. Bautista, R. Schobert and J. Ruiz, Luminescent gold(i) complexes of 1-pyridyl-3-anthracenyl-chalcone inducing apoptosis in Colon carcinoma cells and Antivascular effects, *Inorg. Chem.*, 2019, **58**, 12954–12963.
 - 18 C. R. P. Fulong, S. Kim, A. E. Friedman and T. R. Cook, Coordination-Driven Self-Assembly of Silver(i) and Gold(i) Rings: Synthesis, Characterization, and Photophysical Studies, *Front. Chem.*, 2019, **7**, 567–580.
 - 19 R. Carnelutti, F. D. da Silva, R. Cervo, R. F. Schumacher and E. S. Lang, Gold(i) phosphine complexes with bis(2-pyridyl)diselenoether: Synthesis and structure elucidation, *Inorg. Chem. Commun.*, 2017, **81**, 51–54.
 - 20 N. Svahn, A. J. Moro, C. Roma-Rodrigues, R. Puttreddy, K. Rissanen, P. V. Baptista, A. R. Fernandes, J. C. Lima and L. Rodríguez, The important role of the nuclearity, rigidity, and solubility of phosphanes ligands in the biological activity of gold(i) complexes, *Chem. – Eur. J.*, 2018, **24**, 14654–14667.
 - 21 A. Pinto, C. Cuhna, G. Aullón, J. C. Lima, L. Rodríguez and J. S. Seixas de Melo, Comprehensive Investigation of the Photophysical Properties of Alkynylcoumarin Gold(i) Complexes, *J. Phys. Chem. B*, 2021, **125**, 11751–11760.
 - 22 E. Aguiló, A. J. Moro, R. Gavara, I. Alfonso, Y. Pérez, F. Zaccaria, C. Fonseca Guerra, M. Malfois, C. Baucells, M. Ferrer, J. C. Lima and L. Rodríguez, Reversible self-assembly of water-soluble Gold(i) complexes, *Inorg. Chem.*, 2018, **57**, 1017–1028.
 - 23 A. Pinto, M. Echeverri, B. Gómez-Lor and L. Rodríguez, How to achieve near unity fluorescence quantum yields on gold(i) benzothiadiazole-based derivatives, *Dyes Pigm.*, 2022, **202**, 110308.
 - 24 S. Chakraborty, D. Bhattacharjee and S. A. Hussain, Formation and control of excimer of a coumarin derivative in Langmuir-Blodgett films, *J. Lumin.*, 2014, **145**, 824–831.
 - 25 R. Gavara, J. Llorca, J. C. Lima and L. Rodríguez, A luminescent hydrogel based on a new Au(i) complex, *Chem. Commun.*, 2013, **49**, 72–74.
 - 26 D. Danino, Cryo-TEM of soft molecular assemblies, *Curr. Opin. Colloid Interface Sci.*, 2012, **17**, 316–329.
 - 27 K. Holmberg, B. Jönsson, B. Kronberg and B. Lindman, *Surfactants and polymers in aqueous solution*, John Wiley & Sons, 2nd edn, 2002.
 - 28 A. R. Tehrani-Bagha, J. Kärnbratt, J.-E. Löfroth and K. Holmberg, Cationic ester-containing gemini surfactants: Determination of aggregation numbers by time-resolved fluorescence quenching, *J. Colloid Interface Sci.*, 2012, **376**, 126–132.
 - 29 N. J. Turro and A. Yekta, Luminescent probes for detergent solutions. A simple procedure for determination of the mean aggregation number of micelles, *J. Am. Chem. Soc.*, 1978, **100**, 5951.
 - 30 P. P. Infelta, M. Grätzel and J. K. Thomas, Luminescence decay of hydrophobic molecules solubilized in aqueous micellar systems. Kinetic model, *J. Phys. Chem.*, 1974, **78**, 190.
 - 31 P. P. Infelta, Fluorescence quenching in micellar solutions and its application to the determination of aggregation numbers, *Chem. Phys. Lett.*, 1979, **61**, 88.
 - 32 M. Almgren, F. Grieser and J. K. Thomas, Dynamic and static aspects of solubilization of neutral arenes in ionic micellar solutions, *J. Am. Chem. Soc.*, 1979, **101**, 279.
 - 33 M. Almgren, J.-E. Löfroth and R. Rydholm, Co-existence of rod-like and globular micelles in the ctac-ctac-H₂O system. Evidence from the fluorescence of solubilized pyrene, *Chem. Phys. Lett.*, 1979, **63**, 265.
 - 34 C. Bannwarth, S. Ehlert and S. Grimme, GFN2-xTB-An accurate and broadly parametrized self-consistent tight-binding quantum chemical method with multipole electrostatics and density-dependent Dispersion Contributions, *J. Chem. Theory Comput.*, 2019, **15**, 1652.
 - 35 P. Dey, P. Rajdev, P. Pramanik and S. Ghosh, Specific supramolecular interaction regulated entropically favorable assembly of amphiphilic macromolecules, *Macromolecules*, 2018, **51**, 5182–5190.
 - 36 P. P. N. Syamala, B. Soberats, D. Görl, S. Gekle and F. Würthner, Thermodynamic insights into the entropically driven self-assembly of amphiphilic dyes in water, *Chem. Sci.*, 2019, **10**, 9358–9366.
 - 37 D. Görl and F. Würthner, Entropically driven self-assembly of bolaamphiphilic perylene dyes in water, *Angew. Chem., Int. Ed.*, 2016, **55**, 12094–12098.

- 38 J. Arcau, V. Andermark, E. Aguiló, A. Gandioso, A. Moro, M. Cetina, J. C. Lima, K. Rissanen, I. Ott and L. Rodríguez, Luminescent alkynyl-gold(i) coumarine derivatives and their biological activity, *Dalton Trans.*, 2014, **43**, 4426–4436.
- 39 T. C. Huang, H. Toraya, T. N. Blanton and Y. Wu, X-ray powder diffraction analysis of silver behenate, a possible low-angle diffraction standard, *J. Appl. Crystallogr.*, 1993, **26**, 180–184.
- 40 J. Kieffer and D. Karkoulis, PyFAI, a versatile library for azimuthal regrouping, *J. Phys.: Conf. Ser.*, 2013, 425.
- 41 P. V. Konarev, V. V. Volkov, A. V. Sokolova, M. H. J. Koch and D. Svergun, PRIMUS: a Windows PC-based system for small-angle scattering data analysis, *J. Appl. Crystallogr.*, 2003, **36**, 1277–1282.
- 42 D. I. Svergun, Determination of the regularization parameter in indirect-transform methods using perceptual criteria, *J. Appl. Crystallogr.*, 1992, **25**, 495–503.
- 43 D. Svergun, Restoring low resolution structure of biological macromolecules from solution scattering using simulated annealing, *Biophys. J.*, 1999, **76**, 2879–2886.
- 44 S. Grimme, C. Bannwarth and P. Shushkov, A robust and accurate tight-binding quantum chemical method for structures, vibrational frequencies, and noncovalent interactions of large molecular systems parametrized for all spd-block elements ($Z = 1-86$), *J. Chem. Theory Comput.*, 2017, **13**, 1989.
- 45 R. Ahlrichs, M. Bär, M. Häser, H. Horn and C. Kölmel, Electronic structures calculations on workstation computers: The program system turbomole, *Chem. Phys. Lett.*, 1989, **162**, 165–169.
- 46 A. D. Becke, Density-functional exchange-energy approximation with correct asymptotic behavior, *Phys. Rev. A*, 1988, **38**, 3098–3100.
- 47 J. P. Perdew, Density-functional approximation for the correlation energy of the inhomogeneous electron gas, *Phys. Rev. B: Condens. Matter Mater. Phys.*, 1986, **33**, 8822–8824.
- 48 S. Grimme, J. Antony, S. Ehrlich and H. Krieg, A consistent and accurate ab initio parametrization of density functional dispersion correction (DFT-D) for the 94 elements H-Pu, *J. Chem. Phys.*, 2010, **132**, 154104.
- 49 S. Grimme, S. Ehrlich and L. Goerigk, Effect of the damping function in dispersion corrected density functional theory, *J. Comput. Chem.*, 2011, **32**, 1456.
- 50 F. Weigend and R. Ahlrichs, Balanced basis sets of split valence, triple zeta valence and quadrupole zeta valence quality for H to Rn: Design and assessment of accuracy, *Phys. Chem. Chem. Phys.*, 2005, **7**, 3297–3305.
- 51 D. Andrae, U. Haeussermann, M. Dolg, H. Stoll and H. Preuss, Energy-adjusted ab initio pseudopotentials for the 2nd and 3rd row transition-elements, *Theor. Chim. Acta*, 1990, **77**, 123–141.
- 52 A. Schäfer, A. Klamt, D. Sattel, J. C. W. Lohrenz and F. Eckert, COSMO Implementation in TURBOMOLE: Extension of an efficient quantum chemical code towards liquid systems, *Phys. Chem. Chem. Phys.*, 2000, **2**, 2187–2193.